

Friction velocity estimation using a 2D sonic anemometer in coastal zones

Bernardo FIGUEROA-ESPINOZA^{1,3*}, Zulia SÁNCHEZ-MEJÍA^{2,3}, Jorge Maximiliano UUH-SONDA^{1,3},
Paulo SALLES^{1,3}, Luis MÉNDEZ-BARROSO^{2,3} and Hugo Alberto GUTIÉRREZ-JURADO⁴

¹Laboratorio de Ingeniería y Procesos Costeros, Instituto de Ingeniería, Universidad Nacional Autónoma de México, Puerto de abrigo S/N, 97355, Sisal, Yucatán, México.

²Departamento de Ciencias del Agua y Medioambiente, Instituto Tecnológico de Sonora, 5 de Febrero 818 sur, Col Centro, 85000 Ciudad Obregón, Sonora, México.

³Laboratorio Nacional de Resiliencia Costera (LANRESC), UNAM-CONACYT (www.lanresc.mx).

⁴Department of Earth, Environmental and Resource Sciences, The University of Texas at El Paso, 500 W. University Ave., Geological Sciences Bldg., Room 227-A, El Paso, TX 79968, USA.

*Corresponding author; email: bfigueroae@yahoo.com

Received: August 11, 2020; accepted: March 17, 2021

RESUMEN

La velocidad de fricción (u_*) es un parámetro importante usado en el estudio de flujos geofísicos y de ingeniería. El uso cada vez más frecuente de anemómetros sónicos 2D en estaciones meteorológicas modernas hace que la estimación de u_* a partir de las componentes horizontales de la velocidad sea una posibilidad muy deseable. La presencia de diferentes regímenes de viento (como brisas marinas en zonas costeras) hace que los parámetros turbulentos dependan de la dirección de viento y de la estabilidad atmosférica. Esto hace la estimación de u_* a partir de mediciones 2D muy difícil de obtener. En este trabajo se propone una expresión simple (para u_*) y se valida usando datos provenientes de seis experimentos de campo independientes localizados en zonas costeras. Los resultados muestran que es posible estimar la velocidad de fricción a partir de mediciones 2D (componentes de la velocidad horizontal) usando la intensidad de turbulencia como un proxy de u_* , reduciendo sustancialmente la sensibilidad del estimado a la dirección de viento y estabilidad atmosférica, con bajo error medio cuadrático ($0.06 < \text{RMSE} < 0.097$) y alto coeficiente de correlación ($0.77 < r^2 < 0.95$).

ABSTRACT

Friction velocity (u_*) is an important velocity scale used in the study of engineering and geophysical flows. The widespread use of 2D sonic anemometers in modern meteorological stations makes the estimation of u_* from just the horizontal components of the velocity a very attractive possibility. The presence of different wind regimes (such as sea breezes in or near coastal zones) causes the turbulent parameters to be dependent on the wind direction. Additionally, u_* depends on atmospheric stability, which makes the estimation of u_* from 2D measurements very difficult. A simple expression is proposed, and then tested with data from six independent experiments located in coastal zones. The results show that it is possible to estimate friction velocity from 2D measurements using the turbulence intensity as a proxy for u_* , reducing substantially the sensitivity to the wind direction or atmospheric stability, with small root mean squared errors ($0.06 < \text{RMSE} < 0.097$) and high correlation coefficients ($0.77 < r^2 < 0.95$).

Keywords: friction velocity, Eddy Covariance, Monin-Obukhov Similarity Theory, Sonic Anemometry, 2D anemometer, Coastal Zone.

1. Introduction

Friction velocity is one of the most important scaling parameters in atmospheric sciences and oceanography (Garrat, 1977; Stapleton and Huntley, 1995). Most processes and relationships in the low atmosphere involve the friction velocity, such as turbulent exchange of mass and energy at the surface and relationships based on the Monin-Obukhov Similarity Theory (Monin and Obukhov, 1954; Wyngaard et al., 1977) and on the surface renewal theory (Brutsaert, 1982; Stull, 1988; Castellví, 2018; Castellví et al., 2020). The friction velocity, u_* , is defined as (Stull, 1988):

$$u_* = \left(\overline{u'w'^2} + \overline{v'w'^2} \right)^{1/4} \quad (1)$$

where u , v , and w are the x , y , and z components of the velocity vector; u' , v' and w' are the velocity fluctuations with respect to the mean velocity components U , V , and W (i.e., $u' = u - U$). The overbar refers to time averaging. There are many different definitions of the friction or shear velocity (Weber, 1999) and the selection depends primarily on the particular application. Eq. (1) is related to the length of the Reynolds Stress vector when u is aligned with the mean velocity, hence this definition is independent of the chosen frame of reference and will be used in this report.

There are a variety of techniques to estimate u_* (Champagne et al., 1977; Nieuwstadt, 1978; Durand et al., 1991; Bauer et al., 1992; Inoue et al., 2011; Newman and Klein, 2014). For instance, the eddy covariance (EC) method uses high frequency direct measurement of velocity fluctuations in the surface layer to obtain the friction velocity from Eq. (1) (Burba, 2013). The measurement can be made using hot wire, sonic or other type of anemometer, as long as (a) the three components of the velocity are measured, and (b) the acquisition frequency is large enough to capture the rapid turbulent fluctuations; note that the averaging period must not be too long in order to avoid contamination from slow non-turbulent signals or trends (usually between 30 and 60 min).

Sonic anemometers are convenient because they do not have moving parts (the measurement is based on the speed of sound). Two dimensional (2D) sonic anemometers are much more robust and affordable

than triaxial sonic anemometers. Unfortunately, 2D sonic anemometers cannot be used to directly determine the friction velocity (Eq. 1) because the vertical wind component is not measured; however, an estimate of friction velocity could be obtained from the logarithmic wind profile (Echols and Wagner 1972; Bauer et al., 1992; Bergeron and Abrahams, 1992; Sozzi et al., 1998), but this method requires deployment of 2D anemometers at several heights. In this investigation, a method to estimate friction velocity from a single 2D anemometer is proposed and tested against field measurements.

2. Method

On the basis that the turbulent standard deviation of the horizontal wind speed does not follow similarity and it is well correlated with the friction velocity and the horizontal mean wind speed (Dyer, 1974; Panofsky et al., 1977; Sorbjan, 1987; Stull, 1988; Graefe, 2004; Banerjee et al., 2015), here a semi-empirical relationship is proposed to estimate the friction velocity using a 2D sonic anemometer capable to record (in a half-hourly basis) accurate values of the turbulent standard deviation of the horizontal wind speed and the mean wind speed as follows:

$$\sqrt{\frac{u_{*2D}}{U}} = aI^b \quad (2)$$

$$I = \frac{2\overline{u'^2}}{U^2} \quad (3)$$

where a and b are coefficients that must be calibrated against the friction velocity determined using a triaxial sonic anemometer. Once a and b are known, the friction velocity from 2D measurements (u_{*2D}) can be estimated from Eqs. (2) and (3). Here the velocity vector was rotated in the mean wind direction (i.e., the cross-wind component), thus I is related to the turbulent intensity (Stapleton and Huntley, 1995; Pope et al., 2006; Yahaya and Frangi, 2009). Notice that Eq. (2) can be interpreted as a relationship between a drag coefficient and the turbulence intensity (it can be rewritten as $C_D \sim I^{4b}$), with the inconvenience that the measurements can be done at different heights above ground (see Table I), so it would not be a “standard” drag coefficient, but a local one (Mahrt et al., 2001).

Table I. Characteristics of the experimental sites.

	Sisal meteorological mast (S1)	El Palmar (S2)	Estero el Soldado (S3)	Navopatia (S4)	Cape Tribulation (S5)	Gingin (S6)
Latitude (°)	21.1647	21.0293	27.95	26.3999	-16.1032	-31.3763
Longitude (°)	-89.9533	-90.0637	-110.97	-109.2397	145.4469	115.7138
Type of terrain	Complex, no orography. 100 m from the coastline. Barrier island close to a town	Homogeneous. Tropical dry seasonal forest	Open water, coastal lagoon. Type: Arheic	Flat, homogeneous mangrove close to an estuarine lagoon	Tropical rainforest	Coastal plain woodland on SW Australia
Time-series dates	2010/Jul/29-2012/May/23	2018/Mar/15-2019/Aug/21	2019/Jan/01-2019/Dec/31	2018/Jan/01-2018/Dec/31	2011/Jan/01-2011/Dec/31	2019/Jan/01-2019/Dec/31
Canopy height (m)	Variable	11	0.1	5.0	23	6.8
Roughness length z_0 (m)	Direction-dependent (1^{-6} to $1.5^{-2} \times 10^{-2}$)	0.15	0.015	0.50	0.1 to 1	0.5
Mean wind speed (m s^{-1})	5.77	3.2	2.5	2.42	1.5	3
Dominant wind direction	ESE	ESE	WSW	WSE	SE	SSW and SE
Sensor height to the ground (m)	12.5	21.8	1.8	6.5	45	45
Data set size (number of records)	12 777	16 813	5962	13 253	16 849	14 819

3. Materials and field data

The proposed semi-empirical relationship (Eqs. 2 and 3) was calibrated at six sites with contrasting wind regimes. Table I shows the site locations and experiment characteristics (such as height above ground of the instruments, canopy height, measurement dates, number of records and mean wind speed). Figure 1 shows the map location (upper panel) and the wind roses for each location (lower panel). Note that a different color scale is used in S1 (wind rose) due to its high wind speed average. The site names (and acronyms in parenthesis) are also shown. They are grouped according to their geographical situation in: (1) Gulf of Mexico data sets, (2) Gulf of California data sets, and (3) Australia data sets.

EC experiments must be carefully assessed with statistical data quality tests (Foken and Wichura, 1996; Aubinet et al., 1999). Although most experiments carry out similar pre-processing (peak removal, detrending, gap filling), data quality control is always site-specific. There exist many quality control methods and indexes. Either method can be used with similar results, and stationarity tests are common due to its ease of implementation and interpretation. The method used for each experiment can be consulted in the next section (and references therein). This is important in this context because one cannot use the vertical component of the wind when using a 2D anemometer. However, one can construct stationarity or ogive tests with the horizontal components using the same principles (with the obvious exception of turbulence tests).

All bad data were previously eliminated by the site-specific quality control schemes. We had access to post-processed data using the EC technique (additionally we had raw data from S1 and S2). All sites used a half-hour averaging period. Another aspect of data processing that has to be brought to mind is wind velocity rotation; the post-processed data was already doubly (or triply) rotated, and a 2D measurement can only be rotated in one axis. This subject will be discussed in the last section, where a comparison with single vs. double (and triple) rotation is carried out to assess this issue quantitatively.

3.1 Gulf of Mexico datasets

The first and second experiments are Sisal (S1) and El Palmar (S2), respectively. They are shown in Figure 1a,

both located at the NW of the Yucatan Peninsula in Mexico. S1 is situated at the beach (100 m to the shoreline), to the west end of the town of Sisal; a 50-m height mast equipped with five sonic anemometers at 3, 6, 12.5, 25 and 51 m from the ground was used to acquire wind data between August 2010 and September 2013. Two anemometers (12.5 and 51 m) were 3D (Thies 3.383x) and the rest were 2D (Thies 4.382x). This site is characterized by a bimodal wind speed U regime due to sea breeze (Figueroa-Espinoza et al., 2014). Dominant winds are ESE (seaward) and the average wind speed is 5.77 m s^{-1} at $z = 12.5 \text{ m}$. Even though the terrain is flat, it is non-homogeneous because of the internal boundary layers caused by roughness effects on winds coming from different directions (Figueroa-Espinoza and Salles, 2014; Figueroa-Espinoza et al., 2014). Data pre-conditioning included a triple rotation for 3D anemometers, and single rotation for 2D (Wilczak et al., 2001). Data from a 3D anemometer at height $z = 12.5$ will be used unless specified otherwise. The second site is located 14 km south (inland) of Sisal, in a state reserve called El Palmar (S2 in what follows), a tropical-dry seasonal forest (Fig. 1c; see also Uuh-Sonda et al., 2018, 2021) in flat and homogeneous terrain whose average canopy height ranges from 8 to 12 m. In this site an EC tower is equipped with a WindMaster 3D anemometer at height $z = 21.8 \text{ m}$. Data was post-treated with the EC technique, following Aubinet et al. (1999). A double rotation of the velocity vector was applied for all sites that adhere to this methodology (i.e., S2, S3 and S4) (Delgado et al. 2018; Balbuena et al., 2019; Uuh-Sonda et al., 2021). Prevailing wind directions are EES (Fig. 1d) and, despite being in the range of sea breeze influence (Taylor-Espinosa, 2009; Garza-Pérez and Ize-Lema, 2017), $U_{at} S2 (\sim 3.2 \text{ m s}^{-1}) < U_{at} S1 (5.8 \text{ m s}^{-1})$. S1 data is freely available to the public (Figueroa-Espinoza and Salles, 2020), as well as S2 (Uuh-Sonda et al., 2020).

3.2 Gulf of California datasets

The two coastal sites from the Gulf of California used for this study were (Fig. 1a): Estero el Soldado (S3) and Navopatia (S4). S3 is located in a tidal coastal lagoon in the central region of the Gulf of California (Fig. 1e; Benítez-Valenzuela and Sánchez-Mejía, 2020). S3 has EC instruments including a WindMaster 2329-701-01 3D sonic anemometer

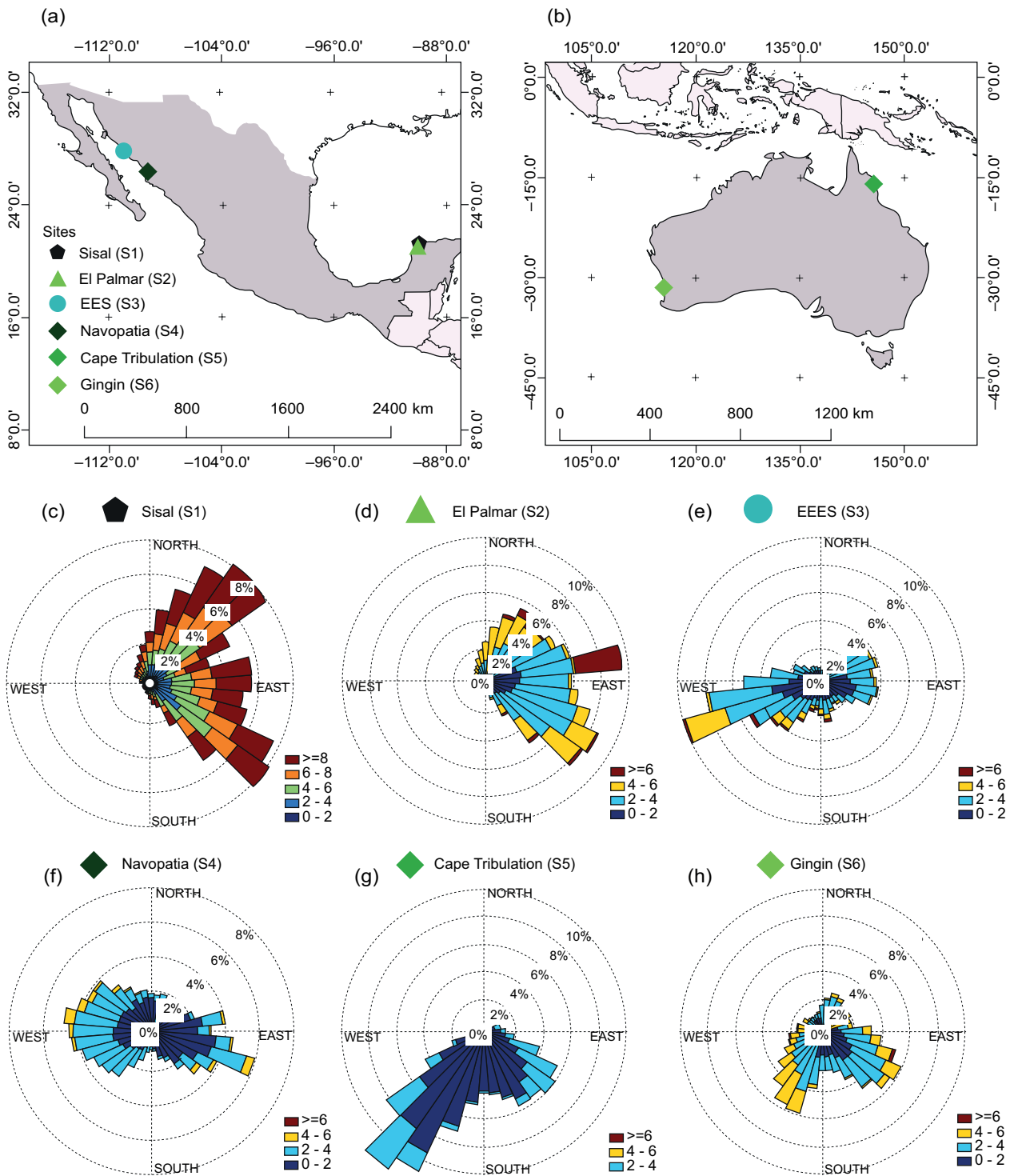


Fig. 1. (a) Location of sites S1, S2, S3, and S4 in Mexico. In the Gulf of California, the site Estero el Soldado (EES, S3-triangle) and Navopatia (S4, dark diamond). To the SE, on the Yucatan Peninsula, El Palmar (S2, green triangle) and Sisal (S1, pentagon). (b) Location of sites S5 and S6 in Australia. In north Queensland, Cape Tribulation (S5, dark green diamond). To the SW, in Western Australia, represented by a green diamond, Gingin (S6). The lower panel shows the wind roses (wind speed in m s^{-1}) for the six experimental sites, together with their respective notation.

deployed on a small floating platform (2×2 m) located at the inlet of the lagoon at 1.8 masl (Barre-ras-Apodaca and Sánchez-Mejía, 2018). Prevailing winds at S3 are WSW (landward; Fig. 1S3), with $U = 2.5 \text{ m s}^{-1}$. EC data for S3 is available at the public repository described in Benítez-Valenzuela et al. (2020). S4 is located within an estuarine system along the northern Mexican Pacific coast (Fig. 1a). It has an EC tower with instruments, including a Windmaster Pro 3D sonic anemometer, sitting 1.5 m above a homogeneous mangrove forest surface (5 m mean canopy height) and has two dominant upwind directions (WSW and SE, Fig. 1f). EC raw data, including 10 Hz U and wind direction for both S3 and S4 was processed using EddyPro software v. 7.0.4 (LI-COR Biosciences, USA). EC data for S4 is available to the public as well (Granados-Martínez et al., 2019).

3.3 Australian datasets

The two coastal sites from the Australian continent included in this study (Fig. 1b) are: (1) the Cape Tribulation flux station (S5) in north Queensland, and (2) the Gingin flux station (S6) in Western Australia. Data from S5 and S6 was graciously provided by Liddell (2013) and Silberstein (2015), respectively, through the Australian Flux Network (OzFlux), where it can be freely accessed. S5 is located within the Daintree Rainforest Observatory between the Coral Sea to the east and a section of the Great Dividing Mountain Range to the west. S5 instruments are mounted on a crane tower at 45 m from the ground in lowland tropical rainforest (25 m average canopy height). Prevailing wind directions in S5 are SE and U is 1.5 m s^{-1} (Fig. 1g). S6 is located on the Swan Coastal Plain (~ 70 km north of Perth) where a flux station equipped with EC and micrometeorological instruments were mounted on a 14 m tall mast inside a native *Banksia* woodland with an irregular canopy (6.8 m average tree height [Silberstein, 2020]). S6 has SW dominant wind directions and U reaching 3 m s^{-1} (Fig. 1h). At both S5 and S6 sites, 10 Hz wind data is measured with CSAT 3D (Campbell Scientific, Logan, UT, USA) sonic anemometers and processed using Py-FLUXPro for data quality control and flux processing (Isaac et al., 2017). For S5, additional processing to the wind data (double rotation) was implemented before the covariance calculation.

4. Wind regimes

Figure 2a-f shows the relationship between friction velocity u_* and the mean horizontal wind speed (2D) U for all the experimental sites (S1 to S6). Instead of using point clouds, we decided to plot a 2D probability histogram (PDF) based on a set of (forty) data bins, so a color scale can tell the regions with more frequency of occurrence.

From Figure 2 it can be inferred that for S1, S3 and S4 (and probably S5) there are two wind regimes due to the sea breeze (direction-dependence). For S1, two straight lines fit data coming from the sea (small slope) and from land (this is very clear in S1). One possibility to estimate the friction velocity would be to perform a linear fit in terms of the streamwise mean wind speed U for each regime, as suggested by Weber (1999), using the corresponding range of directions to identify the different wind regimes when necessary. This procedure works very well, with the inconvenience of having different fit constants for each location and regime (one for winds coming from land and other set of constants for winds coming from the sea, for example). The corresponding values for the linear fit parameters of this exercise for S1 are shown in Table II. Even if the wind coming from the sea may present different behavior depending on the sea state (Charnock, 1955; Wu, 1980; Yahaya and Frangi, 2009), the fit is excellent ($r^2 > 0.79$); however, other locations not so close to the coast would be influenced by the terrain between the coast and the measurement site. Even in S1 the distinction between wind from the sea and from land is not sharp for wind directions aligned ($\pm 10^\circ$) with the shoreline. The data encompasses all atmospheric stabilities, however this calibration would have to be done separately for every location using the wind direction (and a 3D anemometer, for at least one year). Note also that for some sites, such as for S3 and S5, the spread of the data makes very difficult to set a clear-cut criterion for the regime identification, so the method would not be applicable. A method that is insensitive to these wind regimes would be very desirable. The use of the variance instead of the wind speed is intended to achieve regime (and stability) insensitivity, as discussed in the next sections.

5. Results

All experimental data sets include the velocity variance and mean wind speed U . Thus, I can be calculated

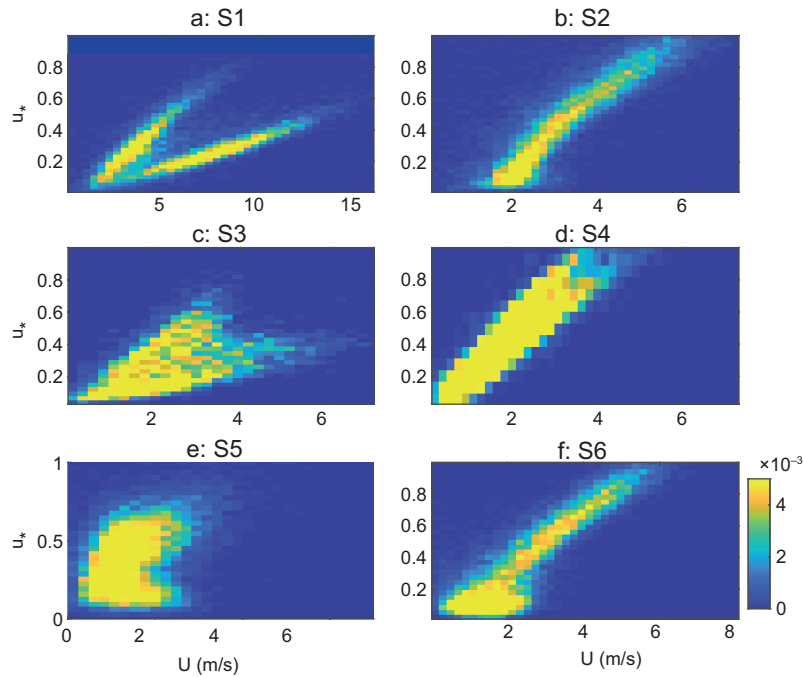


Fig. 2. 2D probability histogram of friction velocity u_* as a function of mean wind speed U (in m s^{-1}) for the six sites.

Table II. Linear fit parameters for site S1 (Sisal), based on u_* vs. U ($u_*2D = p_1U + p_2$) for winds from land and sea (wind speed in m s^{-1}).

Parameter	Sea	Land
p_1	0.03633	0.1018
p_2 (m s^{-1})	-0.0112	-0.0718
r^2	0.7963	0.8614
RMSE	0.0494	0.0659

from Eq. (3) using measured data, and u_{*2D} can be obtained from Eq. (2). Using this simple expression, the best fit parameters (in the least squares sense, comparing to the actual u_* from EC calculations) correspond to $a = 0.5646$ with a 95% confidence interval (CI) in the range (0.5641, 0.5652), and $b = 0.2565$ with a 95% C.I. in the range (0.2558, 0.2572). These parameters are dimensionless.

A comparison of the (3D) u_* and u_{*2D} is shown in Figure 3, again as a 2D probability histogram, for all experimental sites. Titles (a:S1, b:S2 and so on) are indicated on top of each panel. White labels inside each sub-plot indicate goodness of fit parameters (RMSE and r^2). A color scale is shown to the right

of Figure 3f and is the same for all sub-plots. Note that the correlation coefficient ranges from $r^2 = 0.77$ (S5) with RMSE of 0.09 m s^{-1} to $r^2 = 0.95$ (S4) with RMSE of 0.06 m s^{-1} (see also Table III). It is clear that the method based on the turbulent intensity (Eqs. [2] and [3]) succeeded in collapsing the points to a single 1:1 linear relationship for all cases, in spite of the different wind regimes present in S1, S3 and S4 and S5 as well as the atmospheric stability variability. The horizontal variance, as well as I resulted rather insensitive to atmospheric stability (Stull, 1988; Weber, 1999). This was verified using the experimental data and Eq. (2), whose fitting parameters a and b were tabulated on Table IV for different Pasquill-Gifford stability classes (Hall et al., 2000). Both parameters did not vary more than 10% from the values reported in the Method section.

Table III lists the fit coefficients and goodness of fit of the data in Figure 3 (u_* as a function of u_{*2D}). The method works best at S2 and S4, as expected, since these sites do not have dissimilar wind regimes and the terrain and canopy are homogeneous. Interestingly, for S3 the goodness of fit is similar to that of S1.

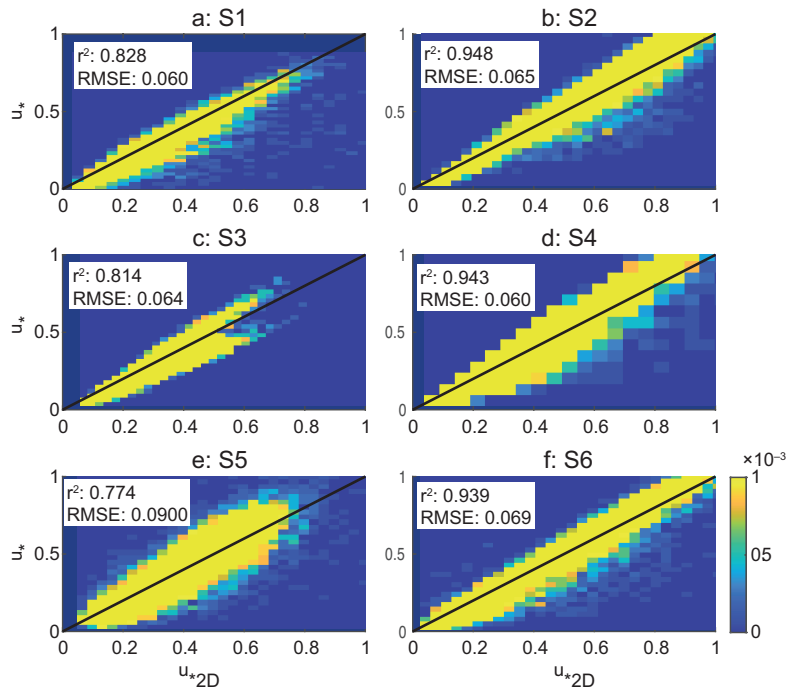


Fig. 3. 2D probability histograms of u^* as a function of u^*_{2D} obtained from Eqs. (2) and (3). Hot colors indicate more frequent data (color bar at the lower right). Goodness of fit parameters are also shown in the white label inside each sub-plot (the thick black line is the 1:1 relationship).

Table III. Fit parameters and goodness of fit for Figure 4a-c (u^* vs. u^*_{2D}). Figures in parentheses are the 95% confidence intervals.

Parameter	S1	S2	S3	S4	S5	S6
p_1	0.8267 (0.819, 0.8345)	0.9527 (0.9487, 0.9567)	0.9757 (0.9649, 0.9865)	1.184 (1.179, 1.189)	0.7956 (0.7884, 0.8028)	0.9291 (0.9246, 0.9336)
p_2 (m s^{-1})	0.04947 (0.04692, 0.05203)	0.00936 (0.007061, 0.01166)	-0.03518 (-0.03913, -0.03124)	$p_2 = -0.05259$ (-0.05496, -0.05021)	0.03299 (0.02938, 0.0366)	-0.008407 (-0.01076, -0.006052)
r^2	0.7738	0.9288	0.8401	0.9429	0.7344	0.9176
RMSE	0.06564	0.07568	0.05911	0.05978	0.0974	0.0800

6. Triple and double rotation vs. single rotation

The purpose of this section is to acknowledge the difference between performing double (or triple) rotation (3D case) and a single rotation (the only possible rotation in a 2D anemometer). The data from most experiments was already averaged using

a 3D rotation scheme. To be more precise, S1 used triple rotation and all other sites used double rotation. Nevertheless, for S1 we actually had 2D anemometers mounted on the mast (at a height of 6 and 25 m), so the estimation can be compared with the 3D case (single rotation vs. triple rotation). Moreover,

Table IV. Fit parameters a and b , and goodness of fit (Eq. [2]) for different Pasquill-Gifford stability classes (Hall et al., 2000).

Stability class	L	a	b	R^2
A	-2	0.528	0.245	0.860
B	-10	0.598	0.282	0.897
C	-100	0.528	0.245	0.860
D	∞	0.587	0.266	0.840
E	100	0.549	0.251	0.838
F	20	0.534	0.255	0.825
G	5	0.542	0.280	0.793

for S5 and S6 we had the full covariance matrix and the rotation angles, so we were able to get a “single rotation covariance matrix” and then calculate u_{*2D} as one would do with a 2D anemometer.

The result of this comparison is shown in Figure 4, where this strictly 2D friction velocity u_{*2D} is compared with the 3D u_* for sites S1 (a), S5 (b) and S6 (c). The goodness of fit (shown inside each sub-figure) can be compared with those of Figure 3: for S1, RMSE increased from 0.066 to 0.067, while r^2 decreased from 0.828 to 0.763. S5 and S6 also show

a slight modification of goodness of fit, as expected, although r^2 improved for S5. If the measurements are carried out on a flat terrain, such as in most coastal zones, and the instruments are well aligned (a bubble level is sufficient to minimize corrections in the vertical), the method can be applied.

Finally, note that for heterogeneous surfaces and contrasting orography, the planar fit method (Wilczak et al., 2001) is recommended. None of the experimental sites present orography (coastal sites) and only S5 presents a relatively tall canopy (~ 20 m, see Table I), so a double rotation would be sufficient for calculating fluxes.

7. Conclusions

A simple power law was proposed to estimate the dimensionless friction velocity $u_* U^{-1}$ using only 2D data (horizontal velocity components) from wind measurements at high acquisition rates (of 10 Hz, in this case). This method of estimation was put to test using experimental data coming from six independent experiments carried out in coastal zones of both northern and southern hemispheres (see Table I). Note that at least three of the sites (S1, S3 and S4)

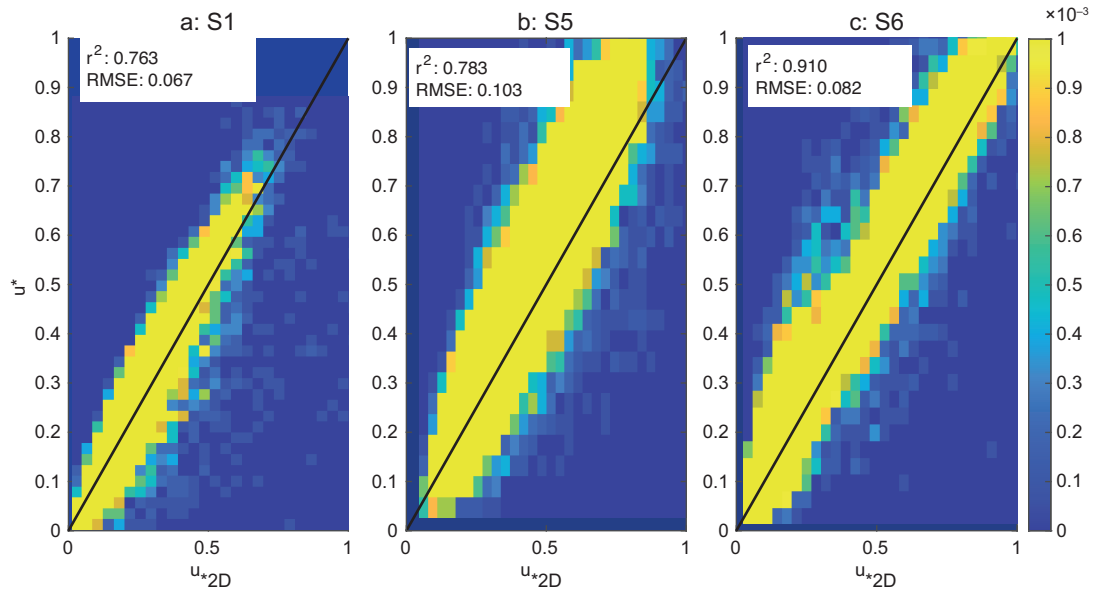


Fig. 4. PDF of actual (3D) friction velocity u_* vs. estimated friction velocity u_{*2D} , obtained from 2D velocity components with single rotation, for the sites (a) S1, (b) S5 and (c) S6. Goodness of fit statistics are shown inside the white labels (the thick black line is the 1:1 relationship).

show two wind regimes due to sea breeze influence, making the estimation a challenging task.

The results show a very good agreement between the 2D estimate of the friction velocity u_{*2D} and u_* (from the 3D EC methodology). The goodness of fit, with $r^2 > 0.77$ in all cases, proves that the methodology can be used at least in flat terrain (homogeneous or complex canopy) like that of coastal zones far from the influence of significant orographic features.

Given the affordability and wide use of 2D anemometers in modern meteorological stations, this study suggests that more estimations of u_* could be carried out by research groups and specialists of different disciplines, particularly in developing countries where 3D anemometry is precluded by the high cost of 3D sonic instruments. Moreover, some sites are located only meters from the shoreline, so the method may also be valid to estimate u_* above the sea surface (or other bodies of water). More research should be carried out in different experimental conditions. In particular, it would be interesting to test (and adapt) the method in complex orography, urban zones and tall and heterogeneous canopies.

Acknowledgments

The authors respectfully acknowledge the support of Laboratorio Nacional de Resiliencia Costera (LAN-RESC LN271544), as well as Consejo Nacional de Ciencia y Tecnología (CONACYT) research grant CONACYT-CFE 89073, CATEDRAS-CONACYT 1146 and CONACYT-SEMARNAT 278608. The technical support of M.Sc. Mariana Gómez-Nicolás, M.Eng. Juan A. Gómez Liera, Dr. José López González, Engr. Gonzalo U. Martín Ruiz, Engr. Lidia I. Benítez Valenzuela, M.Sc. Karol Granados-Martínez and M.Sc. Christian Anibal Silva Ontiveros is also greatly appreciated. We also thank the Comisión de Ecología y Desarrollo Sustentable del Estado de Sonora (CEDES) for granting the research permit to work at the natural protected area Estero el Soldado, and all the park rangers and students. Special thanks to Dr. Alec Torres for the interesting discussions and the motivation to explore the subject of turbulence and friction velocity estimates. We acknowledge Richard Silberstein and Mike Liddell for generously giving us access to the Gingin and

Cape Tribulation datasets. This work used EC data collected by the TERN-OzFlux facility. OzFlux would like to acknowledge the financial support of the Australian Federal Government via the National Collaborative Research Infrastructure Scheme and the Education Investment Fund.

References

- Aubinet M, Grelle A, Ibrom A, Rannik Ü, Moncrieff J, Foken T, Kowalski AS, Martin PH, Berbigier P, Bernhofer Ch, Clement R, Elbers J, Granier A, Grünwald T, Morgenstern K, Pilegaard K, Rebmann C, Snijders W, Valentini R, Vesala T. 1999. Estimates of the annual net carbon and water exchange of forests: The EUROFLUX methodology. *Advances in Ecological Research* 30: 113-175. [https://doi.org/10.1016/S0065-2504\(08\)60018-5](https://doi.org/10.1016/S0065-2504(08)60018-5)
- Balbuena JD, Yépez EA, Pellat FP, Pérez GÁ, Gutiérrez CA, Barrientos MSA, Arredondo T, Niño FA, Bullock SH, Castellanos AE, Cueva A, Figueroa-Espinoza BF, Payán JG, Castillo EGD, Sosa EG, Escobar AG, Hinojo CH, Tha PUK, Celaya CL, Delgado YM, Oechel W, Ruiz ERP, Avendaño MQ, Zazueta CAR, Rodríguez JC, Robles NER, Terrazas TT, Diéguez ET, Uuh-Sonda J, Terminel MLV, Vargas R, Puga MG, Verduzco VS, Vivoni ER, Watts, CJ. 2019. Base de datos de flujos verticales de dióxido de carbono en ecosistemas terrestres y costeros en México. *Elementos para Políticas Públicas* 2: 93-108.
- Banerjee T, Katul GG, Salesky ST, Chamecki M. 2015. Revisiting the formulations for the longitudinal velocity variance in the unstable atmospheric surface layer. *Quarterly Journal of the Royal Meteorological Society* 141: 1699-1711. <https://doi.org/10.1002/qj.2472>
- Barreras-Apodaca A., Sánchez-Mejía ZM. 2018. Eddy covariance observations of semiarid seagrasses from the Gulf of California. In: *Proceedings of the AGU Fall Meeting, Washington DC*, 10-14.
- Bauer BO, Sherman DJ, Wolcott JF. 1992. Sources of uncertainty in shear stress and roughness length estimates derived from velocity profiles. *The Professional Geographer* 44: 453-464. <https://doi.org/10.1111/j.0033-0124.1992.00453.x>
- Benítez-Valenzuela LI, Sánchez-Mejía ZM. 2020. Observations of turbulent heat fluxes variability in a semiarid coastal lagoon (Gulf of California). *Atmosphere* 11: 626. <https://doi.org/10.3390/atmos11060626>

- Benítez-Valenzuela LI, Sánchez-Mejía ZM, Silva-Oniveros CA, Barreras-Apodaca A. 2020. Turbulent fluxes and tide measurements from a coastal lagoon in the Gulf of California. PANGAEA. <https://doi.org/10.1594/PANGAEA.918686>
- Bergeron NE, Abrahams AD. 1992. Estimating shear velocity and roughness length from velocity profiles. *Water Resources Research* 28: 2155-2158. <https://doi.org/10.1029/92WR00897>
- Brutsaert W. 1982. Mean profiles and similarity in a stationary and horizontally-uniform ABL. In: *Evaporation into the atmosphere: Theory, history, and applications*. Springer, Dordrecht, 57-112.
- Burba G. 2013. Eddy covariance method for scientific, industrial, agricultural and regulatory applications: A field book on measuring ecosystem gas exchange and areal emission rates. LI-COR Biosciences.
- Castellví F. 2018. An advanced method based on surface renewal theory to estimate the friction velocity and the surface heat flux. *Water Resources Research* 54: 10-134. <https://doi.org/10.1029/2018WR022808>
- Castellví F, Medina ET, Cavero Campo J. 2020. Surface eddy fluxes and friction velocity estimates taking measurements at the canopy top. *Agricultural Water Management* 241: 106358. <https://doi.org/10.1016/j.agwat.2020.106358>
- Champagne FH, Friehe CA, LaRue JC, Wynagaard JC. 1977. Flux measurements, flux estimation techniques, and fine-scale turbulence measurements in the unstable surface layer over land. *Journal of Atmospheric Sciences* 34: 515-530. [https://doi.org/10.1175/1520-0469\(1977\)034%3C0515:FMFE-TA%3E2.0.CO;2](https://doi.org/10.1175/1520-0469(1977)034%3C0515:FMFE-TA%3E2.0.CO;2)
- Charnock H. 1955. Wind stress on a water surface. *Quarterly Journal of the Royal Meteorological Society* 81: 639-640. <https://doi.org/10.1002/qj.49708135027>
- Delgado-Balbuena J, Yépez EA, Paz-Pellat F, Ángeles-Pérez G, Aguirre-Gutiérrez C, Arredondo T, Alvarado-Barrientos MS, et al. 2018. Base de datos de flujos verticales de dióxido de carbono en ecosistemas terrestres y costeros en México. *Elementos para Políticas Públicas* 2: 93-108.
- Durand P, De Sa L, Druilhet A, Said F. 1991. Use of the inertial dissipation method for calculating turbulent fluxes from low-level airborne measurements. *Journal of Atmospheric and Oceanic Technology* 8: 78-84. [https://doi.org/10.1175/1520-0426\(1991\)008%3C0078:UOTIDM%3E2.0.CO;2](https://doi.org/10.1175/1520-0426(1991)008%3C0078:UOTIDM%3E2.0.CO;2)
- Dyer A. 1974. A review of flux-profile relationships. *Boundary-Layer Meteorology* 7: 363-372. <https://doi.org/10.1007/BF00240838>
- Echols WT, Wagner NK. 1972. Surface roughness and internal boundary layer near a coastline. *Journal of Applied Meteorology* 11: 658-662. [https://doi.org/10.1175/1520-0450\(1972\)011%3C0658:SRAIBL%3E2.0.CO;2](https://doi.org/10.1175/1520-0450(1972)011%3C0658:SRAIBL%3E2.0.CO;2)
- Figueroa-Espinoza B, Salles P, Zavala-Hidalgo J. 2014. On the wind power potential in the northwest of the Yucatan Peninsula in Mexico. *Atmósfera* 27: 77-89.
- Figueroa-Espinoza B, Salles P. 2014. Local Monin-Obukhov similarity in heterogeneous terrain. *Atmospheric Science Letters* 15: 299-306. <https://doi.org/10.1002/asl2.503>
- Figueroa-Espinoza B, Salles P. 2020. Wind velocity vertical profile in a 50 m wind mast at Sisal, Yucatán, Mexico [data set]. Zenodo. <http://doi.org/10.5281/zenodo.3923126>
- Foken Th, Wichura B. 1996. Tools for quality assessment of surface-based flux measurements, *Agricultural and Forest Meteorology* 78: 83-105. [https://doi.org/10.1016/0168-1923\(95\)02248-1](https://doi.org/10.1016/0168-1923(95)02248-1)
- Garratt JR. 1977. Review of drag coefficients over oceans and continents. *Monthly Weather Review* 105: 915-929. [https://doi.org/10.1175/1520-0493\(1977\)105%3C0915:RODCOO%3E2.0.CO;2](https://doi.org/10.1175/1520-0493(1977)105%3C0915:RODCOO%3E2.0.CO;2)
- Garza-Pérez JR, Ize-Lema IAR. 2017. Caracterización multidisciplinaria de la zona costera de Sisal, Yucatán. Laboratorio Nacional de Resiliencia Costera, Yucatan, Mexico. Available at: http://www.sisal.unam.mx/labeco/LAB_ECOLOGIA/Produccion_academica_de_Xavier_files/ZONA%20COSTERA%20SISAL.pdf (accessed on May 3, 2020).
- Graefe J. 2004. Roughness layer corrections with emphasis on SVAT model applications. *Agricultural and Forest Meteorology* 124: 237-251. <https://doi.org/10.1016/j.agrformet.2004.01.003>
- Granados-Martínez KP, Méndez-Barroso LA, Rivas Marquez JA 2019. Navopatia flux station eddy covariance (EC) data (2017-2019). PANGAEA. <https://doi.org/10.1594/PANGAEA.905663>
- Hall DJ, Spanton AM, Dunkerley F, Bennett M, Griffiths RF. 2000. An Inter-comparison of the AERMOD, ADMS and ISC dispersion models for regulatory applications. R&D Technical Report P362. Environment Agency, Bristol, UK, 80 pp.
- Inoue T, Glud RN, Stahl H, Hume A. 2011. Comparison of three different methods for assessing in situ friction

- velocity: A case study from Loch Etive, Scotland. *Limnology and Oceanography: Methods* 9: 275-287. <https://doi.org/10.4319/lom.2011.9.275>
- Isaac P, Cleverly J, McHugh I, Van Gorsel E, Ewenz C, Beringer J. 2017. OzFlux data: Network integration from collection to curation. *Biogeosciences* 14: 2903-2928. <https://doi.org/10.5194/bg-14-2903-2017>
- Liddell M. 2013. Cape Tribulation OzFlux tower site. Data from the Cape Tribulation site, Far North Queensland. OzFlux. Australian and New Zealand Flux Research and Monitoring. hdl: 102.100.100/14242
- Mahrt L, Vickers D, Sun J, Jensen NO, Jørgensen H, Pardyjak E, Fernando H. 2001. Determination of the surface drag coefficient. *Boundary-Layer Meteorology* 99: 249-276. <https://doi.org/10.1023/A:1018915228170>
- Monin AS, Obukhov AM. 1954. Basic laws of turbulent mixing in the surface layer of the atmosphere. *Tr. Akad. Nauk. SSSR Geophys. Inst.* 24: 163-187.
- Newman JF, Klein PM. 2014. The impacts of atmospheric stability on the accuracy of wind speed extrapolation methods. *Resources* 3: 81-105. <https://doi.org/10.3390/resources3010081>
- Nieuwstadt F. 1978. The computation of the friction velocity u^* and the temperature scale T^* from temperature and wind velocity profiles by least-square methods. *Boundary-Layer Meteorology* 14: 235-246. <https://doi.org/10.1007/BF00122621>
- Panofsky H, Tennekes H, Lenschow D, Wyngaard J. 1977. The characteristics of turbulent velocity components in the surface layer under convective conditions. *Boundary-Layer Meteorology* 11: 355-361. <https://doi.org/10.1007/BF02186086>
- Pope ND, Widdows J, Brinsley MD. 2006. Estimation of bed shear stress using the turbulent kinetic energy approach—A comparison of annular flume and field data. *Continental Shelf Research* 26: 959-970. <https://doi.org/10.1016/j.csr.2006.02.010>
- Stull RB. 1988. An introduction to boundary layer meteorology. Kluwer Academic Publishers, The Netherlands.
- Silberstein R. 2015. Gingin OzFlux: Australian and New Zealand Flux Research and Monitoring. hdl: 102.100.100/22677. Available at: <http://data.ozflux.org.au/portal/home.jsp> (accessed on June 4, 2020).
- Silberstein R. 2020. Personal communication.
- Sorbjan Z. 1987. An examination of local similarity theory in the stably stratified boundary layer. *Boundary-Layer Meteorology* 38: 63-71. <https://doi.org/10.1007/BF00121555>
- Sozzi R, Favaron M, Georgiadis T. 1998. Method for estimation of surface roughness and similarity function of the wind speed vertical profile. *Journal of Applied Meteorology* 37: 461-469. [https://doi.org/10.1175/1520-0450\(1998\)037<0461:MFEOS-R>2.0.CO;2](https://doi.org/10.1175/1520-0450(1998)037<0461:MFEOS-R>2.0.CO;2)
- Stapleton KR, Huntley DA. 1995. Seabed stress determinations using the inertial dissipation method and the turbulent kinetic energy method. *Earth Surface Processes and Landforms* 20: 807-815. <https://doi.org/10.1002/esp.3290200906>
- Taylor-Espinoza N. 2009. Análisis y visualización de la componente diurna de los vientos en el sur del Golfo de México. B.Sc. thesis. Facultad de Ciencias, UNAM, Mexico. Available at: <http://132.248.9.195/ptd2009/marzo/0640679/Index.html>
- Uuh-Sonda JM, Gutiérrez-Jurado HA, Figueroa-Espinoza B, Méndez-Barroso LA. 2018. On the ecohydrology of the Yucatan Peninsula: Evapotranspiration and carbon intake dynamics across an eco-climatic gradient. *Hydrological Processes* 32: 2806-2828. <https://doi.org/10.1002/hyp.13230>
- Uuh-Sonda JM, Figueroa-Espinoza B, Gómez-Nicolás MP, Gómez-Liera J. 2020. Wind observations in a 22 m tower at El Palmar state reserve, Yucatan, Mexico [data set]. Zenodo. <https://doi.org/10.5281/zenodo.3975261>
- Uuh-Sonda JM, Figueroa-Espinoza B, Gutiérrez-Jurado HA, Méndez-Barroso LA. 2021. Ecosystem productivity and evapotranspiration dynamics of a seasonally dry tropical forest of the Yucatan Peninsula. *Journal of Geophysical Research*. Under review.
- Weber RO. 1999. Remarks on the definition and estimation of friction velocity. *Boundary-Layer Meteorology* 93: 197-209. <https://doi.org/10.1023/A:1002043826623>
- Wilczak JM, Oncley SP, Stage SA. 2001. Sonic anemometer tilt correction algorithms. *Boundary-Layer Meteorology* 99: 127-150. <https://doi.org/10.1023/A:1018966204465>
- Wu J. 1980. Wind-stress coefficients over sea surface near neutral conditions—A revisit. *Journal of Physical Oceanography* 10: 727-740. [https://doi.org/10.1175/1520-0485\(1980\)010<0727:WSCOSS>2.0.CO;2](https://doi.org/10.1175/1520-0485(1980)010<0727:WSCOSS>2.0.CO;2)
- Wyngaard JC, Coté OR, Izumi Y. 1971. Local free convection, similarity, and the budgets of shear stress and heat flux. *Journal of the Atmospheric Sciences* 28: 1171-1182. [https://doi.org/10.1175/1520-0469\(1971\)028<1171:LFCSAT>2.0.CO;2](https://doi.org/10.1175/1520-0469(1971)028<1171:LFCSAT>2.0.CO;2)

Yahaya S, Frangi JP. 2009. Profile of the horizontal wind variance near the ground in near neutral flow—K-theory and the transport of the turbulent kinetic energy.

Annales Geophysicae 27: 1843-1859. <https://doi.org/10.5194/angeo-27-1843-2009>